Title	Viscoelastic modeling of Zircaloy cladding in-pile transient creep
Author(s)	Tulkki, Ville; Ikonen, Timo
Citation	Journal of Nuclear Materials. Elsevier. Vol. 457 (2015), Pages 324 - 329
Date	2014
URL	http://dx.doi.org/10.1016/j.jnucmat.2014.11.100
Rights	Post-print version of the article. This article may be downloaded for personal use only.

Viscoelastic modeling of Zircaloy cladding in-pile transient creep

Ville Tulkki*, Timo Ikonen

VTT Technical Research Centre of Finland, P.O.Box 1000, 02044 VTT Finland

Abstract

In fuel behaviour modelling accurate description of the cladding stress response is important for both operational and safety considerations. The cladding creep determines in part the width of the gas gap, the duration to pellet-cladding contact and the stresses to the cladding due to the pellet expansion. Conventionally the strain hardening rule has been used to describe the creep response to transient loads in engineering applications. However, it has been well documented that the strain hardening rule does not describe well results of tests with load drops or reversals.

In our earlier work we have developed a model for primary creep which can be used to simulate the in- and out-of-pile creep tests. Since then several creep experiments have entered into public domain. In this paper we develop the model formulation based on the theory of viscoelasticity, and show that this model can reproduce the new experimental results. We also show that the creep strain recovery encountered in experimental measurements can be explained by viscoelastic behaviour.

Keywords: Zircaloy, creep, stress transient, Standard Linear Solid, viscoelastic

1. Introduction

The cladding tube of nuclear fuel rod protects the urania pellets from the corrosive environment as well as contains the radioactive fission products. Early on during the rod reactor life the cladding creeps inwards due to pressure differential between the reactor system pressure and the rod fill gas. The inward creep of the cladding and swelling of the fuel pellet eventually lead to closing of the gas gap and mechanical interaction between pellets and cladding wall. And with very high burnup there is the possibility of high rod internal pressure exceeding the system pressure, potentially causing the cladding creep outwards faster than the pellets swell and re-opening the gas gap. All these affect the fuel performance and some have potential to cause fuel failures. It is therefore very important to properly understand and describe the various phenomena affecting the fuel rod. While numerous studies have been done on the creep properties of various cladding materials [1, 2, 3, 4, 5, 6, 7, 8, 9, 10, 11, 12, 13], the creep response to transient stresses is investigated only in a small subset of the work [1, 2, 5, 8, 10, 12]. However it should be noted that the transient response governs the cladding behaviour during situations where most damage can happen, i.e. transients.

Conventionally fuel cladding deformation is assumed to have elastic and viscoplastic components. Viscoplastic creep is described by having three regions: the primary (or transient) region, the secondary steady state region and the third leading to failure. The correlations are matched to experiments with a single stress increase, and the change of stress encountered in fuel behaviour analysis is handled by hardening laws. The creep in metals is assumed to follow either a time or a strain hardening law, and the latter is believed to hold for Zirconium alloys in usual operating conditions [2].

Various creep correlations have been formulated over the years that take both thermal and irradiation creep into account. It is well known that the hardening laws used to take the transient conditions into account are simplifications and do not apply universally. Stress reversal and stress reduction are special situations where the hardening law fails and requires additional assumptions to model the observed behaviour [1, 2, 5]. These situations have been successfully described with complex formulations of cladding material thermodynamic states [14, 15] and by assuming additional deformation terms such as reversible anelastic deformation [1, 16]. Also anisotropy of the cladding tubes can be described with high precision with advanced methods [7, 17].

*Tel. +358 20 722 6114; fax +358 20 722 7001.
E-mail address: ville.tulkki@vtt.fi

While these formulations appear to provide correct prediction of the cladding creep behaviour they are not commonly implemented in fuel behaviour codes due to their complexity and computational limitations [18]. Fuel behaviour analysis is commonly performed with integral codes utilizing separate models to describe various phenomena, and the number of required simulations may rise to hundreds of thousands of fuel rod simulations depending on the application [19]. For this purpose, a simple and more practical approach is needed. Previously we have shown that the cladding behaviour during stress reversal and reduction can be roughly modelled using simple internal variable approach [20].

In this paper we develop the primary creep model further starting from Standard Linear Solid model which is commonly used in studies of viscoelasticity of a wide range of materials and as such provides a solid theoretical foundation for the model. We compare the primary creep model to experimental data that has recently entered the public domain. The model with primary creep based on viscoelastic behaviour is derived in Section 2. Halden experiments IFA-699 and IFA-696 are are used to assess the validity of the model in Section 3 and the results are discussed in Section 4. Conclusions are given in Section 5.

2. Creep model

2.1. Viscoelastic model

In studies of viscoelastic properties of solids, a common method of describing models is via so-called mechanical analogs [21]. These combine springs representing the elastic component of the material to dashpots representing the viscous components. The springs' displacement is $\epsilon_{\text{spring}} = \sigma/\kappa_i$, where κ_i is the elastic modulus of spring i and σ is the external stress affecting the given component, while the dashpots' rate of displacement is of $\dot{\epsilon}_{\text{dashpot}} = \sigma/\eta_i$, where η_i is the viscosity of the dashpot i. Other components are also possible in order to describe more complex interactions.

A mechanical analog of our creep model is shown in Fig. 1. There is a separate node describing the secondary thermal and irradiation creep in series to a Standard Linear Solid (SLS) model. Secondary creep is nonlinear [4, 7, 6, 22] yet it interacts with rest of the system similarly to dashpot as it is decoupled from the elastic and primary creep deformations in creep experiments. Therefore the dashpot symbol D is used as a stand-in for a more complex function describing the secondary creep. SLS consists of two parallel arms, a spring and a serial combination of a spring and a dashpot. The SLS is the simplest mechanical analog cabable of qualitatively describing material behaviour during both imposed stress (so-called creep tests) and imposed elongation (stress relaxation test) [21].

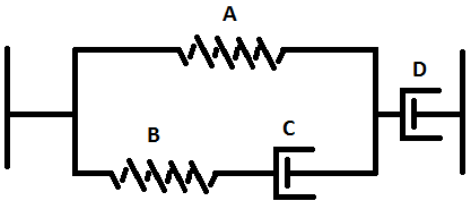

Figure 1: Mechanical analog for the Standard Linear Solid model (nodes A, B and C) in series with a node D representing secondary creep contribution.

Conventionally the stress response of the cladding is separated into elastic response ϵ_{el} and creep, which in turn has both primary (ϵ_p) and secondary (ϵ_s) components:

$$\epsilon = \epsilon_{el} + \epsilon_p + \epsilon_s. \tag{1}$$

SLS part of the model shown in Fig. 1 simulates the elastic and primary creep components of Eq. (1) and replaces the need for strain hardening rule. It should be evident from Fig. 1 that the elastic response and primary creep are instrinctly linked in this formulation and the secondary creep is separate, in contrast to most formulations [4, 7, 6] which consider primary and secondary creep linked and elastic response separate from the creep.

The solution to SLS is well known [21]. The general relationship is given by

$$\sigma(t) + \frac{\eta_C}{\kappa_B}\frac{d\sigma(t)}{dt} = \kappa_A\left(\epsilon(t) + \eta_C\frac{\kappa_A+\kappa_B}{\kappa_A\kappa_B}\frac{d\epsilon(t)}{dt}\right), \tag{2}$$

where either the strain ϵ or stress σ can be solved when the other is given as well as the initial condition is known.

In the context of fuel behaviour modelling we are interested in solving the strain as a function of piece-wise constant stress that can be implemented into the time-stepping scheme of the fuel performance code. For simplicity, we assume that the stress in the beginning is zero, $\sigma(t_0) \equiv \sigma_0 = 0$, and the strain correspondingly $\epsilon_0 \equiv \epsilon(t_0) = 0$. Further, we assume that the stress changes occur instantaneously at times t_i so that for $t_i \leq t < t_{i+1}$ the stress is constant $\sigma(t) = \sigma(t_i) \equiv \sigma_i$. Then the stress can be written as

$$\sigma(t) = \sum_{i=1}^{N} \Delta\sigma_i \Theta\left(t - t_i\right), \tag{3}$$

where $\Delta\sigma_i = \sigma_i - \sigma_{i-1}$, Θ is the Heaviside step function and the sum is taken over all the N stress changes.

The solution of the SLS model is derived in Appendix A. The resulting strain including the elastic, primary creep and secondary creep contributions is of the form

$$\epsilon(t) = \frac{\sigma(t)}{\kappa} + C\sum_{i=1}^{N}\Delta\sigma_i\left(1 - e^{-\frac{t-t_i}{\tau}}\right)\Theta(t-t_i) + \int_{t_0}^{t} f(\sigma(\xi))\,d\xi, \quad (4)$$

with the constants given by

$$\kappa = \kappa_A + \kappa_B, \quad (5)$$

$$C = \frac{\kappa_B}{\kappa_A(\kappa_A + \kappa_B)}, \quad (6)$$

$$\tau = \eta_C \frac{\kappa_A + \kappa_B}{\kappa_A \kappa_B}. \quad (7)$$

The first term in Eq. (4) corresponds to the elastic strain, the second to primary creep and the last one to secondary creep (both thermal and irradiation induced).

2.2. Implementation of model for primary creep

The primary creep term,

$$\epsilon_p(t) = C\sum_{i=1}^{N}\Delta\sigma_i\left(1 - e^{-\frac{t-t_i}{\tau}}\right)\Theta(t-t_i), \quad (8)$$

involves a sum over the whole stress history with exponentially decaying contributions from all the previous stress changes. In such a non-Markovian form the model is difficult to implement into a fuel performance code. However, it is possible to write the model in a form where the future evolution of the system depends only on the present state of the system. This can be done by introducing an additional variable describing the internal state of the system where the memory effects can be embedded.

We describe the internal state of the cladding with a single time-dependent stress-like variable $\sigma_{\text{int}}(t)$. The time evolution $\sigma_{\text{int}}(t)$ describes the relaxation of the internal state of the system towards the steady state determined by the applied stress $\sigma(t)$. The scale of $\sigma_{\text{int}}(t)$ is chosen so that for an initial state with zero primary creep rate and the applied stress equal to σ_0, $\sigma_{\text{int}}(t_0) = \sigma_0$. As the applied stress is changed to σ_1, the variable $\sigma_{\text{int}}(t)$ starts to evolve in time, approaching the new steady state value $\sigma_{\text{int}}(t \to \infty) = \sigma_1$, which is reached when the primary creep has fully saturated. For several stepwise changes as in Eq. (3), the model takes the form (see Appendix A and Ref. [20])

$$\epsilon_p(t + \Delta t) = \epsilon_p(t) + C\left[\sigma(t) - \sigma_{\text{int}}(t)\right]\left(1 - e^{-\frac{\Delta t}{\tau}}\right), \quad (9)$$

$$\sigma_{\text{int}}(t + \Delta t) = \sigma(t) - \left[\sigma(t) - \sigma_{\text{int}}(t)\right]e^{-\frac{\Delta t}{\tau}}. \quad (10)$$

The model yields a primary creep that is reinitiated at each stress change and whose saturated value is proportional to the change in stress. These are in line with observations from experiments conducted at Halden Reactor [12, 23]. The evolution in time is a simple exponential function which would correspond to a single relaxation mechanism. While this is probably not the case for Zirconium based alloys used in cladding tubes [1, 4], we consider the simplicity of the model and presentation to be important at this point. Previously we have shown the creep model using Eqs. (9) and (10) to be able to describe the creep behaviour during step stress transients [20] in experiments conducted by Matsuo [5] and in IFA-585 experiment performed in Halden research reactor [12, 24, 25]. More complex variations of SLS exist [21] and these should be utilized to model the exact time evolution of the primary creep.

2.3. Implementation of model for secondary creep

The secondary creep is a complex phenomenon and much research has been dedicated to determining the factors affecting it, see e.g. Refs [3, 4, 6, 13, 12, 22]. Fortunately in our model the secondary creep is fully decoupled from the elastic and primary creep contributions in creep experiment conditions. For simulating the secondary steady state contribution to creep we use fuel performance code FRAPCON-3.4's correlation [26, 27, 28] which is effectively the model by Limbäck and Andersson [6] modified to use effective stress σ_{eff} instead of hoop stress:

$$\dot{\epsilon}_{th} = A\frac{E}{T}(\sinh\frac{a_i\sigma_{\text{eff}}}{E})^n e^{-\frac{Q}{RT}} \text{ and} \quad (11)$$

$$\dot{\epsilon}_{irr} = C_0 \cdot \phi^{C_1} \cdot \sigma_{\text{eff}}^{C_2} \cdot f(T), \quad (12)$$

where E is the elastic modulus, T is temperature in K, R is the universal gas constant, Q the activation energy of the creep, ϕ the fast neutron flux (n/m^{2}s^{-1}) and variables A, a_i, n, C_i and the function $f(T)$ have different values depending on the cladding type and the environment as described in Ref. [28]. The use of σ_{eff}

$$\sigma_{\text{eff}} = \sqrt{0.5((\sigma_a - \sigma_h)^2 + (\sigma_h - \sigma_r)^2 + (\sigma_r - \sigma_a)^2)} \quad (13)$$

is justified by an improved modelling of tensile and compressive creeps [28]. Here $\sigma_{a,h,r}$ denote stresses in axial, hoop and radial directions and isotropic behaviour is assumed for simplicity.

3. Experimental verification

3.1. IFA-699

Recently Halden Work Report HWR-882 [23] was declassified. It describes the experiment IFA-699 featuring on-line measurements of the creep of Zircaloy-4, E110, M5 and M-MDA cladding tube segments containing fuel pellets for realistic temperature gradient. The experiment was still on-going but at the time it had lasted for nearly 3000 full power hours and had subjected the cladding samples to hoop stress levels of 0, -75, -50 and +30 MPa of hoop stress, with negative values indicating compression and positive values tension. This was achieved by alternating the segment internal pressure (to 18.2, 8.5, 11.6 and 22.7 MPa) while the external pressure was at steady 16.2 MPa simulating PWR conditions.

We compare the model with the measurements of Zircaloy-4 segment as the secondary creep model is tuned for it. In order to simulate the experiment, the effective mid-wall stress σ_{eff} was calculated from

$$\sigma_{\text{eff}} = \sqrt{3}\frac{(p_{\text{int}} - p_{\text{ext}})r_i^2 r_o^2}{((r_i + r_o)/2)^2(r_o^2 - r_i^2)} \tag{14}$$

where r_i and r_o are the cladding tube inner and outer radii and p_{int} and p_{ext} the pressures internal and external to the tube. The fast flux was reported to be $1.5 \cdot 10^{13}$ n/cm^2/s and cladding temperature approximately 625 K [23]. Primary creep coefficients $C = 5 \times 10^{-6}$ m^2/N and $\tau = 40$ h were fitted to match the experimental data. The measured values are shown as dots and the base simulation as the solid line in Fig. 2.

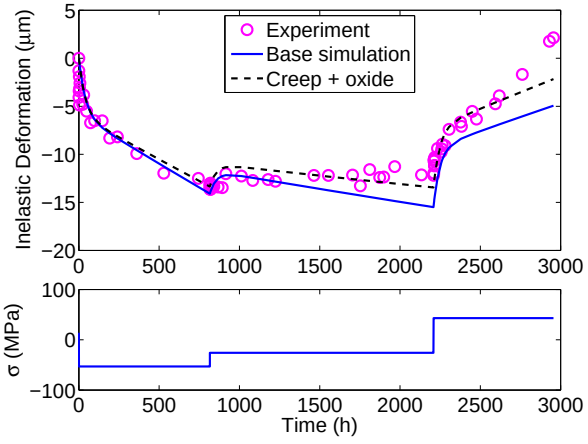

Figure 2: Creep of Zircaloy-4 segment in IFA-699 experiment, with measurements shown in circles and simulated values with lines.

The measured values in Fig. 2 consistently trend toward the positive (or tensile, outward) direction. One possible explanation would be that the general stress is not the correct driving force for creep. It should be noted that the original correlation [6] using hoop stress as a driving force yields a worse match between creep in tension and compression. Third contender for the driving force is the deviatoric hoop stress as suggested by Foster and Baranwal [29]. Other possibility is the growth of oxide layer which did complicate the interpretation of the earlier Halden experiment [12]. We included a oxide growth contribution to the simulations according to Eq. (15) [30]

$$\delta = Ke^{-\frac{E}{RT}}t^n \tag{15}$$

where δ is the oxide layer thickness in μm assuming a constant temperature, $K = 23663.76\ \mu m \cdot h^{-1}$, $E/R = 8645.4$ K, $T = 625$ K is the interaction layer temperature, t is time in hours and $n = 1.02474$. As the oxidation replaces metal with less dense oxide, the net effect is the increase of the apparent diameter by a fraction of one third of the oxide layer thickness. The creep with oxide layer contribution is shown with dashed line in Fig. 2. This case would represent a situation where the Zircaloy-4 segment is heated by the fuel inside and thus oxidises faster than the measurement calibration piece which we assume would be at coolant temperature (approximately 50 K lower than the test sample). The used oxide layer equation is a simple formula fitted to publicly available post-irradiation data for PWR fuels with Zircaloy-4 cladding, and as such caution should be used when utilizing it for samples in Halden flask conditions.

While there are uncertainties regarding the secondary creep and the effect of oxidation on the measurements it should be noted that these do not affect the primary creep part of the model which performs well in describing the experimental results.

3.2. IFA-696

A creep experiment with Zircaloy-2 specimens was conducted at Halden reactor and reported by Kozar et al. [22]. They reported witnessing a contraction of a sample during a period of very low stress at reactor operational temperatures and flux. Models following the traditional strain hardening rule do not predict such a behaviour. This contraction is well known, as for instance Limbäck and Andersson describe the need to quickly cool the test samples after depressurization in order to avoid the recovery of creep strain in their experiments [6]. However, according to our model this contraction is to be expected and can be explained by viscoelastic behaviour. In the case of the behaviour corresponding to our proposed model the rate of the elon-

gation would be similar in both cases, just in opposite directions.

Data points were taken from Figures 4 and 5 of Ref. [22] representing the measured deformation during the initial creep and during the zero-stress period. The absolute values of deformation for both cases are shown in Fig. 3 clearly demonstrating that both the rate and the scale of the creep are the same, therefore supporting the assumption that the viscoelastic behaviour is responsible for the sample contraction.

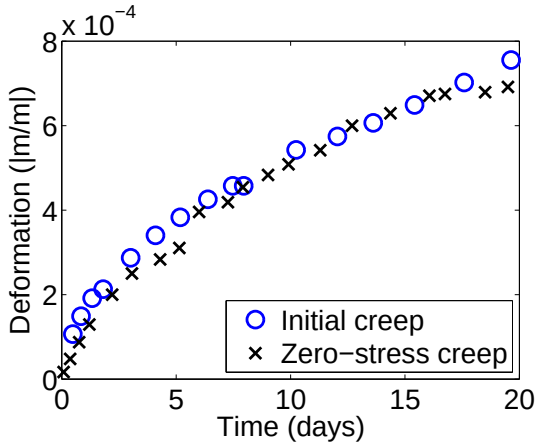

Figure 3: Magnitude of deformation during the initial creep and the zero-stress period for Zircaloy-2 sample in IFA-696 experiment [22].

4. Discussion

The major difference of the model presented in this paper to the conventional approach is that we separate the deformation into viscoelastic and viscoplastic components instead of using the usual approach to separate elastic and viscoplastic (creep) components. The viscoelastic component is modelled with Standard Linear Solid model which is known to be able to model the behaviour of various substances for small deformations. As this limitation is also inherent in the 1D approach for cladding modelling in engineering level codes, it should not decrease the usability domain of the fuel performance codes.

Similar approaches to cladding creep have been proposed by Murty [1] and Geelhood [31]. Murty adds an anelastic component to the usual elastic and creep components [1], thus indicating that a part of the transient deformation is due to delayed elasticity (or viscoelasticity). In contrast to this our model describes the whole of transient deformation by viscoelasticity. The reason to this difference might be the difference in in- and ex-pile behaviour. Murty investigates cladding creep in out-of-pile experiments and as we saw in our previous work [20] it would appear that the in-pile creep differs quantitatively from out-of-pile creep. Geelhood presents a model with a stress threshold for re-initiation of the primary creep [31] to explain the observations of IFA-699. While our approach provides similar results with stress steps that are long enough for the primary creep to fully develop, the viscoelastic model is more consistent in situations with rapid stress changes.

The SLS-based model is able to replicate the creep behaviour of IFA-699 creep experiment's Zircaloy-4 segment. In earlier work [20] the similar approach was shown to be able to describe the behaviour of earlier IFA-585 experiment [12, 24, 25] as well as out-of-pile Zircaloy-4 creep experiment with load drops and reversals by Matsuo [5]. The used time constant $\tau = 40$ h was the same as the one describing out-of-pile Zircaloy-4 primary creep whereas the $C = 5 \times 10^{-6}$ m^2/N is lower than for the out-of-pile tests. This might be due to the higher temperature (by approximately 30 K) or significantly higher stress levels (potentially leaving linear stress response regime) used in Matsuo's experiments. While the experimental conditions do not exactly match each other, there are similarities in the time evolution and stress dependancy of primary creep. This would indicate that the irradiation would not have a strong effect on primary creep. There are challenges in modelling the steady state creep behaviour with the chosen model for secondary creep. There may be several explanations: the usual variation in creep behaviour between different Zircaloy tubes, the general stress not being the proper driving force for the creep or the effect of differing oxide formation rates.

The observed contraction during the stress-free period at operating temperatures of IFA-696 [22] is similar in magnitude to the initial primary creep. This is as expected should the viscoelastic behaviour accurately describe the Zircaloy stress response, whereas traditional strain hardening law requires additional assumptions to be made. The match between creep at the beginning of the experiment and during the stress-free period is surprisingly good as one would expect secondary creep to show during the tensile creep. This feature may stem from several sources. For instance, temperature fluctuated between 530–550 K during the zero-stress creep period, thus potentially influencing the measurements. Also, as the data is provided only as a relative deformation the elastic deformation may affect the reference level. This would slightly increase the apparent magnitude of inwards creep.

Kozar et al. investigate the reason to observed con-

traction based on calculated reaction rates [22]. According to their analysis, irradiation-induced transient creep would be too rapid to account for the observed contraction, and therefore they deduce that the relaxation of strain-hardening of the microstructure is the likely reason to the observations. We would claim instead that the observed contraction is due to the viscoelastic properties of the material. It could be argued that these two interpretations are just different expressions for the same phenomenon, however the difference becomes evident when behaviour during change in stress direction is considered. Under such conditions our model based on SLS behaves in a way that is supported by the observations of earlier Halden experiments [8, 12, 23].

5. Conclusions

The cladding tube creep response to transient stresses is traditionally modelled according to strain hardening law in engineering level integral fuel behaviour codes. This approach has severe limitations in modelling of situations with load reductions and reversals. Also, additional postulated phenomena such as creep recovery have been introduced to account for the experimental observations. In this paper we have derived a creep model based on the theory of viscoelasticity. We have shown that it can be used to model the observed transient creep phenomena on an empirical macroscopic level as well as provide interpretation on the experimentally observed creep strain recovery phenomenon.

While conventionally nuclear fuel cladding deformation has been considered to consist of elastic and viscoplastic components, our analysis demonstrates that viscoelastic behaviour should also be considered. This influences cladding response to transient conditions, and therefore has implications to analysis of phenomena such as pellet cladding interaction and lift-off.

Acknowledgements

This work was partially funded by SAFIR2014, the Finnish Research Programme on Nuclear Power Plant Safety 2011-2014, and Academy of Finland funded IDEA project.

Appendix A. Derivation of the SLS solution and the primary creep algorithm

The elastic and primary creep terms in Eq. (4) can be solved from the general form of the SLS solution [Eq. (2)] by substituting for $\sigma(t)$ the piece-wise constant stress function of Eq. (3), and $d\sigma(t)/dt = \sum_{i=1}^{N} \Delta\sigma_i \delta(t - t_i)$ for the time derivative. Here $\delta(t-t_i)$ is the Dirac delta distribution. This results in the equation

$$\kappa_A \epsilon + \kappa_A \tau \frac{d\epsilon}{dt} = \sum_{i=1}^{N} \Delta\sigma_i \Theta(t - t_i) + \frac{\eta_C}{\kappa_B} \sum_{i=1}^{N} \Delta\sigma_i \delta(t - t_i).$$

The strain ϵ can be solved by taking the Laplace transform $\hat{\epsilon}(s) = \int_{t_0}^{t} \epsilon(t') e^{st'} dt'$, and assuming the initial condition $\epsilon(t_0) = 0$. Then, one has

$$\kappa_A (1 + \tau s)\hat{\epsilon}(s) = \sum_{i=1}^{N} \left[\Delta\sigma_i e^{-st_i} \left(\frac{1}{s} + \frac{\eta_C}{\kappa_B} \right) \right],$$

which, after re-arranging gives

$$\hat{\epsilon}(s) = \frac{1}{\kappa_A} \sum_{i=1}^{N} \left\{ \Delta\sigma_i e^{-st_i} \left[\frac{1}{s} + \left(\frac{\eta_C}{\kappa_B \tau} - 1 \right) \frac{1}{s + 1/\tau} \right] \right\}.$$

Inverse Laplace transform of $\hat{\epsilon}(s)$ gives

$$\begin{aligned}
\epsilon(t) &= \sum_{i=1}^{N} \left[\Delta\sigma_i \Theta(t - t_i) \left(\frac{1}{\kappa_A} - \frac{\kappa_B}{\kappa_A(\kappa_A + \kappa_B)} e^{-\frac{t-t_i}{\tau}} \right) \right] \\
&= \frac{1}{\kappa_A + \kappa_B} \sum_i \Delta\sigma_i \Theta(t - t_i) + \\
&\quad + \frac{\kappa_B}{\kappa_A(\kappa_A + \kappa_B)} \sum_{i=1}^{N} \Delta\sigma_i \left[1 - e^{-\frac{t-t_i}{\tau}} \right] \Theta(t - t_i) \\
&= \frac{\sigma(t)}{\kappa} + C \sum_{i=1}^{N} \Delta\sigma_i \left(1 - e^{-\frac{t-t_i}{\tau}} \right) \Theta(t - t_i),
\end{aligned}$$

with C given by Eq. (6). The primary creep of Eq. (8) is then identified as the second term,

$$\epsilon_p(t) = C \sum_{i=1}^{N} \Delta\sigma_i \left(1 - e^{-\frac{t-t_i}{\tau}} \right) \Theta(t - t_i).$$

Force balance implies that the stress imposed on the SLS (A, B, C) and the secondary creep (D) parts of the model shown in Fig. 1 are equal. Therefore the strain due to secondary creep can be simply added to the strain of the SLS part, as is done in Eq. (4).

To derive the algorithm of Eqs. (9) and (10), we first use Eq. (8) to write down $\epsilon_p(t + \Delta t)$, then divide the sum over stress changes into two parts: those changes occurring before time t, and those occurring between t

and $t + \Delta t$:

$$\epsilon_p(t+\Delta t) = C\sum_{i=1}^{N}\Delta\sigma_i\left(1-e^{-\frac{t+\Delta t-t_i}{\tau}}\right)\Theta\left(t+\Delta t-t_i\right)$$
$$= C\sum_{i=1}^{N}\Delta\sigma_i\left(1-e^{-\frac{t+\Delta t-t_i}{\tau}}\right)\Theta\left(t-t_i\right)+$$
$$+ C\sum_{i=1}^{N}\Delta\sigma_i\left(1-e^{-\frac{t+\Delta t-t_i}{\tau}}\right)\Theta\left(t+\Delta t-t_i\right)\Theta\left(t_i-t\right)$$

If the length of the time step Δt is chosen such that the stress is constant between t and $t + \Delta t$, the last term is equal to zero. In this case,

$$\epsilon_p(t+\Delta t) = C\sum_{i=1}^{N}\Delta\sigma_i\left(1-e^{-\frac{t+\Delta t-t_i}{\tau}}\right)\Theta\left(t-t_i\right)$$
$$= C\sum_{i=1}^{N}\Delta\sigma_i\left(1-e^{-\frac{t-t_i}{\tau}}\right)\Theta\left(t-t_i\right)e^{-\frac{\Delta t}{\tau}}+$$
$$- C\sum_{i=1}^{N}\Delta\sigma_i\left(1-e^{-\frac{\Delta t}{\tau}}\right)\Theta\left(t-t_i\right)e^{-\frac{\Delta t}{\tau}}$$
$$= \epsilon_p(t)e^{-\frac{\Delta t}{\tau}} + C\sigma(t)\left(1-e^{-\frac{\Delta t}{\tau}}\right)+\left[\epsilon_p(t)-\epsilon_p(t)\right]$$
$$= \epsilon_p(t)+\left[C\sigma(t)-\epsilon_p(t)\right]\left(1-e^{-\frac{\Delta t}{\tau}}\right)$$

To derive the form of the algorithm used in this work, we introduce the internal stress variable $\sigma_{\text{int}}(t)$ as $C\sigma_{\text{int}}(t) = \epsilon_p(t)$. Hence, from Eq. (8),

$$\sigma_{\text{int}}(t) = \sum_{i=1}^{N}\Delta\sigma_i\left(1-e^{-\frac{t-t_i}{\tau}}\right)\Theta\left(t-t_i\right).$$

Repeating the steps shown for ϵ_p above, one gets

$$\sigma_{\text{int}}(t) = \sigma_{\text{int}}(t)e^{-\frac{\Delta t}{\tau}} + \sigma(t)\left(1-e^{-\frac{\Delta t}{\tau}}\right).$$

By re-arranging terms, the primary creep algorithm is then obtained as

$$\epsilon_p(t+\Delta t) = \epsilon_p(t) + C\left[\sigma(t)-\sigma_{\text{int}}(t)\right]\left(1-e^{-\frac{\Delta t}{\tau}}\right),$$
$$\sigma_{\text{int}}(t+\Delta t) = \sigma(t) - \left[\sigma(t)-\sigma_{\text{int}}(t)\right]e^{-\frac{\Delta t}{\tau}}.$$

We note that one may use the above derivation to write down a mathematically equivalent algorithm without introducing the internal stress variable σ_{int}. An equivalent algorithm to Eqs. (9) and (10) would be, for instance,

$$\epsilon_p(t+\Delta t) = \epsilon_p(t)e^{-\frac{\Delta t}{\tau}} + C\sigma(t)\left(1-e^{-\frac{\Delta t}{\tau}}\right).$$

Finally, we recall that both forms of the algorithm rely on the assumption of constant stress over the time step Δt. To take into account the stress change occurring at t_i, one would need to take small time steps δt that bound the stress change as $t \le t_i \le t + \delta t$, and derive the corresponding equations for updating ϵ_p. However, it can be shown that the correction due to this additional step goes to zero in the limit of small δt. That is, $\epsilon_p(t + \delta t) = \epsilon_p(t)$ as $\delta t \to 0$ even when the stress changes between t and $t + \delta t$. In practice one can ignore this intermediate step and change the value of $\sigma(t)$ at the beginning of each time step Δt.

References

[1] K. Murty, K. Yoon, Transactions of the 5th International Conference on Structural Mechanics in Reactor Technology (SMiRT-5) C3/6 (1979).
[2] G. Lucas, R. Pelloux, Nuclear Technology 53 (1981) 46–57.
[3] D. Franklin, G. Lucas, A. Bement, ASTM STP 815 (1983).
[4] Y. Matsuo, Journal of Nuclear Science and Technology 24 (1987) 111–119.
[5] Y. Matsuo, ASTM STP 1023 (1989) 678–691.
[6] M. Limback, T. Andersson, ASTM STP 1295 (1996) 448–468.
[7] P. Delobelle, P. Robinet, P. Geyer, P. Bouffioux, Journal of Nuclear Materials 238 (1996) 135–162.
[8] M. McGrath, Proceedings of the 2000 International Topical Meeting on LWR Fuel Performance (2000).
[9] A. Soniak, N. L'Hullier, J.-P. Mardon, V. Rebeyrolle, P. Bouffioux, C. Bernaudat, ASTM STP 1423 (2002) 837–862.
[10] K. Ito, K. Kamimura, Y. Tsukuda, Proceedings of the 2004 International Meeting on LWR Fuel Performance (2004) 440–451.
[11] J. Moon, P. Cantonwine, K. Anderson, S. Karthikeyan, M. Mills, Journal of Nuclear Materials 353 (2006) 177–189.
[12] J. Foster, M. McGrath, Proceedings of the 2007 LWR Fuel Performance Meeting (2007).
[13] R. Holt, Journal of Nuclear Materials 372 (2008) 182–214.
[14] D. Lee, F. Zaverl, E. Plaza-Meyer, Journal of Nuclear Materials 88 (1980) 104–110.
[15] L. Jernkvist, Transactions of the 15th International Conference on Structural Mechanics in Reactor Technology (SMiRT-15) C04/3 (1999) 477–484.
[16] K. Murty, JOM 51 (1999) 32–39.
[17] F. Onimus, J.-L. Bechade, Journal of Nuclear Materials 384 (2009) 163–174.
[18] M. Rautenberg, D. Poquillon, P. Pilvin, C. Grosjean, J. Cloue, X. Feaugas, Nuclear Engineering and Design 269 (2014) 33–37.
[19] T. Ikonen, V. Tulkki, Nuclear Engineering and Design 275 (2014) 229–241.
[20] V. Tulkki, T. Ikonen, Journal of Nuclear Materials 445 (2014) 98–103.
[21] H. Banks, S. Hu, Z. Kenz, Advances in Applied Mathematics and Mechanics 3 (2011) 1–51.
[22] R. Kozar, A. Jaworski, T. Webb, R. Smith, Journal of Nuclear Materials 444 (2014) 14–22.
[23] S. Hanawa, HWR-882 (2008).
[24] M. McGrath, HWR-471 (1996).
[25] IFPE database NEA IFPE/IFA-585 experimental data, . Last modified 13-MAR-2008.
[26] K. Geelhood, Nuclear Engineering and Technology 43 (2011) 509–522.
[27] K. Geelhood, W. Luscher, C. Beyer, NUREG/CR-7022, Vol.1 (2011).
[28] W. Luscher, K. Geelhood, NUREG/CR-7024 (2011).

[29] J. Foster, R. Baranwal, 16th ASTM Zirconium Symposium (2010).
[30] J. Katto, Corrosion and its modeling in nuclear reactor fuel cladding, 2013. M.Sc thesis.
[31] K. Geelhood, Proceedings of the 2013 International Topical Meeting on LWR Fuel Performance (2013).